One- and two-photon absorption spectra of dibenzoterrylene

Z. S. Sadeq,* Rodrigo A. Muniz, and J. E. Sipe
Department of Physics, University of Toronto, 60 St. George Street, Toronto, Ontario, Canada M5S 1A7

(Received 15 March 2018; published 19 July 2018)

Dibenzoterrylene (DBT) has garnered interest as a potential single-photon source. To have a better grasp of any possible limitations of using DBT for this application, a better understanding of its optical properties is needed. We use a configuration interaction method to calculate the many-body wave functions of DBT and we use these wave functions to calculate its optical properties. We calculate the linear absorption spectrum and the spatial distributions of electrons involved in several bright transitions. We also calculate the two-photon absorption spectrum of DBT and show that there are several excited states that are bright due to two-photon absorption. Except at high photon energies, we predict that there are no competing optical processes regarding the use of DBT as a single-photon source. Our calculations provide details of the optical properties of DBT that are interesting in general and useful for considering optical applications of DBT.

DOI: 10.1103/PhysRevMaterials.2.075202

I. INTRODUCTION

Single-photon sources are an important resource for optical based quantum information processing [1–7]. Candidate devices are based on semiconductor quantum dots [8–11], color centers in diamond [12–14], and trapped atoms (or ions) in the gas phase [15–17]. Organic materials at cryogenic temperatures also can act as a source of single photons; typically, the optical coherence lifetimes of the relevant transitions in organic materials are longer by an order of magnitude than those of semiconductor quantum dots [3,18–20]. Synthesis of organic materials is relatively straightforward [21–23]; they are simple to deposit on optical chips and waveguides [24]. Thus organic materials open up the possibility of using existing integrated chip strategies to carry out a variety of nonlinear optical processes [25].

Dibenzoterrylene (DBT) is an organic material of interest for a variety of optical applications [26–28], most notably as a possible single-photon source [18–20,25,29–37]. DBT consists of carbon and hydrogen atoms bonded together in a hexagonal structure; it can be thought of as a small graphene flake. Similar to the optical response of graphene, the optical response of DBT is largely determined by the π electrons occupying the p_z orbitals on the carbon atoms. A ball-and-stick representation of the optimized structure of DBT is shown in Fig. 1. Typically, DBT is deposited in an anthracene matrix [25,38], primarily to guard against oxidation and photobleaching, as these processes limit the photostability of the system. DBT has a purely electronic zero phonon line around 785 nm. At low temperatures, the phonon induced dephasing of the transition dipole of the ground state to the first bright excited state, which is labeled S_1, vanishes [39]; the spectral linewidth of this transition is then limited only by the radiative lifetime, and DBT can act as a two level system, similar to a trapped atom [3].

The development of DBT as a single-photon source requires a detailed understanding of its electronic states. In particular, one hindrance in using DBT as a single-photon source is its intersystem crossing, where the population of a singlet state is funneled to a triplet state [18]. The rate at which intersystem crossing proceeds is exponentially suppressed by the energy difference between the singlet and triplet states [41–43], and therefore the energy of the triplet state is important in considering the use of DBT as a single-photon source. There is no consensus on the energy of the first triplet state of DBT, primarily due to experimental limitations. Some researchers have calculated this triplet state to have an energy as low as 0.23 eV above the ground state [44]. This calculated energy is very different from that of the triplet states in the -acenes, materials of similar structure to DBT, which typically have triplet energies on the order of 1 eV above the ground state [45,46].

There are multiple strategies for calculating the energy of the electronic states of DBT, including density matrix renormalization group (DMRG) [47–49] and density functional theory (DFT) [44,50,51]. While there have been DMRG studies on the electronic states of systems with similar structure to DBT [47,48], no calculations have been performed on DBT. Calculations based on methods such as DFT can exhibit large variations in the predicted energies [44,52]. Crucially, these approaches make it difficult to get a simple picture of the electronic behavior in the excited states. Earlier [53], we used the Pariser-Parr-Pople (PPP) model [54–57] to describe the electronic and optical properties of graphene flakes of similar size and structure to DBT. The PPP model is semiempirical; it depends on a small set of parameters to model physical processes, such as the electron hopping and the Coulomb interaction, and it has been successfully implemented to study a range of carbon based materials, from pentacene [47] to graphene flakes [53,58]. In this paper, we use this same model to elucidate the electronic excited states of DBT. One attractive feature of our approach is its ability to provide a simple physical picture of the electronic behavior in these states. We calculate the linear and nonlinear optical absorption of DBT and the electron densities involved in several bright transitions. We demonstrate that there is no other competing one-photon absorption process near the S_1 absorption, and that there are

*sadeqz@physics.utoronto.ca

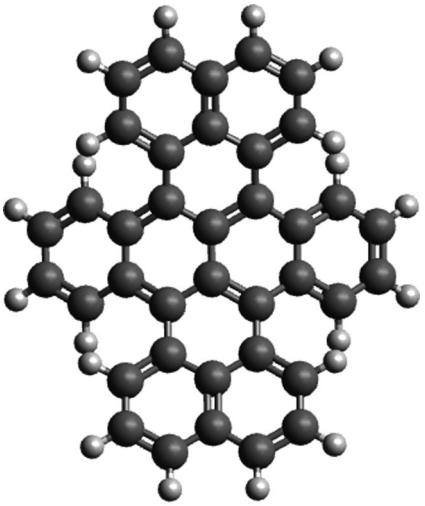

(a)

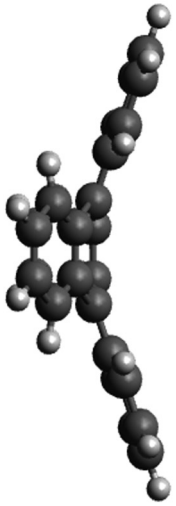

(b)

FIG. 1. Ball-and-stick representation of the optimized structure of DBT, showing both (a) the top view and (b) the side view of the system. We acquired the optimized structure of DBT from the PubChem archive [40].

no optical processes that might hinder the application of DBT as a single-photon source.

This paper is written in four parts. In Sec. II we discuss the model used to describe the electronic states of DBT, in Sec. III we compute the one-photon and two-photon absorption of DBT and the spatial distribution of the electrons involved in several bright transitions, and in Sec. IV we present our conclusions.

II. MODEL AND METHODS

In the optimized structure of a DBT molecule, the atoms do not lie in a plane [19]; the molecule is not flat, but "buckled" (see Fig. 1). Optical applications involve DBT molecules embedded in an anthracene matrix, and how the anthracene matrix affects the structure of a DBT molecule has not been rigorously determined. For simplicity, we assume that the

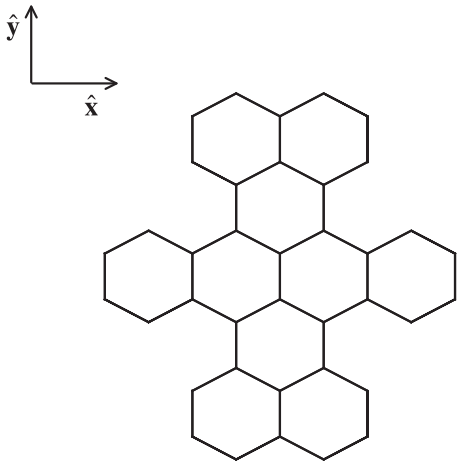

FIG. 2. Skeletal representation of the flat structure of DBT; in this representation, the hydrogen atoms are not shown. The two axes, labeled $\hat{\mathbf{x}}$ and $\hat{\mathbf{y}}$, are used to facilitate discussions.

structure of the DBT molecule is flat, with the carbon atoms in the x, y plane. We assume that the bond lengths (l_b) are uniform throughout the molecule, and we set all bond lengths to $l_b = 1.42$ Å; the bond lengths of the buckled structure of the DBT molecule are similar to the bond lengths of the flat structure [19]. A skeletal representation of the flat structure of DBT is shown in Fig. 2.

We model the p_z electrons in DBT using the Pariser-Parr-Pople (PPP) Hamiltonian [47,53–57],

$$H = H_{\mathrm{TB}} + H_{\mathrm{Hu}} + H_{\mathrm{ext}}, \tag{1}$$

where H_{TB} is the tight-binding Hamiltonian, H_{Hu} is the Hubbard Hamiltonian, and H_{ext} is the extended Hubbard Hamiltonian,

$$H_{\mathrm{TB}} = -\sum_{\langle i,j\rangle,\sigma} t_{ij} c^{\dagger}_{i\sigma} c_{j\sigma}, \tag{2}$$

$$H_{\mathrm{Hu}} = U \sum_{i} n_{i\uparrow} n_{i\downarrow}, \tag{3}$$

$$H_{\mathrm{ext}} = \frac{1}{2} \sum_{\substack{i\neq j \\ \sigma\sigma'}} V_{ij} \left(n_{i\sigma} - \frac{1}{2}\right)\left(n_{j\sigma'} - \frac{1}{2}\right). \tag{4}$$

Here σ is a spin label, i and j are site labels, and the angular brackets indicate sums over nearest neighbors only. The hopping parameter is set to $t_{ij} = 2.66$ eV for the π conjugated bonds and $t_{ij} = 2.22$ eV for the single bonds [48,59,60]. The fermion creation and annihilation operators are denoted respectively by $c^{\dagger}_{i\sigma}$ and $c_{i\sigma}$, so the electron number operator for spin σ and site i is $n_{i\sigma} = c^{\dagger}_{i\sigma} c_{i\sigma}$. The Hubbard repulsion parameter U corresponds to the interaction of electrons on the same site, and V_{ij} extends the Coulomb interaction between electrons at sites i and j. We approximate the long-range Coulomb repulsion by the Ohno interpolation [54],

$$V_{ij} = \frac{U}{\sqrt{1 + (4\pi\epsilon_0 U \epsilon r_{ij}/e^2)^2}}, \tag{5}$$

where ϵ is a screening parameter, r_{ij} is the distance between sites i and j, $e = -|e|$ is the electronic charge, and ϵ_0 is the

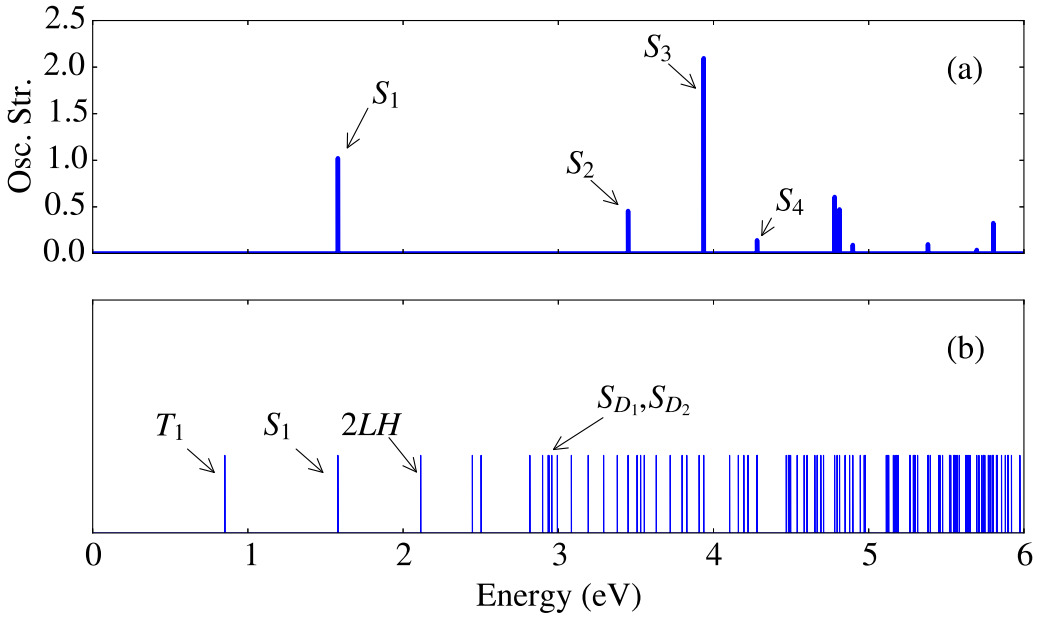

FIG. 3. (a) Plot of the absolute oscillator strengths of the bright transitions and (b) the energies of the excited states above the ground state of DBT. The parameters of our calculation are set such that the S_1 state is 1.58 eV above the ground state in energy. Our calculation predicts that the T_1 state is 0.85 eV above the ground state in energy. The plot of the energies of the excited states above the ground state indicates that there are no other states below the S_1 state in energy besides the T_1 state. The first absorption peak, due to $GS \rightarrow S_1$, has an associated transition dipole moment which is polarized along the $\hat{\mathbf{y}}$ axis. There are several other high energy absorption peaks, the strongest of which is due to $GS \rightarrow S_3$; this transition has a transition dipole moment which is polarized along the $\hat{\mathbf{x}}$ axis. However, these bright states are all more than 3 eV above the ground state in energy, which is around twice the energy of the $GS \rightarrow S_1$ transition. The axes are shown in Fig. 2.

vacuum permittivity. We set $\epsilon = 5$ for all calculations, as this value has been used to study similar systems such as graphene flakes [53,54,58,61]. The Hubbard repulsion parameter is set to $U = 5.88$ eV for all calculations; this choice of U ensures that the first singlet transition energy matches the experimental value, and is similar to the values that have been used to model the p_z electrons in other organic systems [53,54,58]. Measurements of the first singlet transition energy of DBT were carried out on DBT molecules embedded in an anthracene matrix [3,25]. Thus the Hubbard U and the screening parameter ϵ that we employ should be understood as empirically taking into account the effect of the anthracene medium on the energies of the electronic states of DBT. We have chosen the parameters of our semiempirical model [54,62] such that the calculated first singlet transition energy matches its experimental value [63].

We first consider the Hartree-Fock (HF) approximation for the PPP Hamiltonian taking paramagnetic expectation values. The HF approximation for the PPP Hamiltonian is given in Eq. (8) of our earlier work [53]; for DBT, the impurity term is set to zero and the hopping parameter is site dependent. The single-particle states obtained from solving the HF equations are then used to construct the HF ground state. We then rewrite the total Hamiltonian (1) in an electron-hole basis. To solve for the many body wave functions of the system, we restrict the many body Hamiltonian (1) to a set of states following the configuration interaction (CI) method: we employ a basis consisting of the HF ground state and HF single and double excitations. We then diagonalize the many body Hamiltonian (1) restricted to the selected states to obtain the many body wave functions. Upon diagonalization of the many body Hamiltonian, the CI ground state and the CI excited states are superpositions of the HF ground state and the HF excited states. The details of the electron hole basis, and the CI strategy used to solve for the many body wave functions, can be found in our earlier work [53]. For the rest of this paper, we shall refer to the HF single-particle states as "modes," and we shall refer to states that result from the CI calculation simply as "states."

States and transitions of interest

We label the first four bright excited states in ascending energy as the S_n states, where $n = \{1, 2, 3, 4\}$. For the application of DBT as a single-photon source, the transition from the ground state to the S_1 state, denoted $GS \rightarrow S_1$, is the transition of interest; the relaxation of the excitation from the S_1 state to the GS is the source of single photons [25]. We label the lowest energy two-photon active state as the $2LH$ state; this state is primarily composed of a HF double excitation that excites two electrons from the highest occupied HF mode to the lowest unoccupied HF mode. The next two two-photon active states in order of increasing energy are labeled as S_{D_1} and S_{D_2}; these states are composed mainly of HF single excitations. We denote the first triplet state as T_1. The electronic population in the S_1 state can decay to the T_1 state via intersystem crossing [43]; the energy of the T_1 state is important as it represents a source of loss for the single-photon source application. The energies of these states above the ground state are shown in the plot in Fig. 3(b).

Linear optical response

We report the predicted strength of each one-photon absorption peak in terms of the absolute oscillator strength associated with the corresponding transition. The predicted

absolute oscillator strength of the absorption peak due to the transition from the ground state to the state Y [64], denoted by $GS \rightarrow Y$, is

$$f_{Yg} = \frac{2m_e\omega_{Yg}|\boldsymbol{\mu}_{Yg}|^2}{3\hbar e^2}, \tag{6}$$

where m_e is the electron mass, ω_{Yg} is the frequency difference between the state Y and the ground state, $\hbar$ is the reduced Planck's constant, and $\boldsymbol{\mu}_{Yg}$ is the matrix element of the dipole moment operator between the ground state and the state Y. The dipole moment operator was defined in Eq. (21) of our earlier work [53]

We define the "spatial profile" of the transition $GS \rightarrow Y$ as a function $\mathcal{T}_{Y;i}$ of site i given by

$$\mathcal{T}_{Y;i} = \langle Y|n_i|GS\rangle, \tag{7}$$

where GS is the ground state, i is the site, Y is an excited state, and n_i is the number operator for site i; n_i was defined in Eq. (18) of our earlier work [53]. The quantity $\mathcal{T}_{Y;i}$ is related to the matrix element of the dipole moment operator between the ground state and the state Y, the "transition dipole moment,"

$$\langle Y|\boldsymbol{\mu}|GS\rangle = \sum_i e\mathbf{r}_i\mathcal{T}_{Y;i}, \tag{8}$$

where the sum is over all sites i, $\mathbf{r}_i$ is the position of site i, and $\boldsymbol{\mu}$ is the dipole moment operator; $\boldsymbol{\mu}$ was defined in Eq. (21) in our earlier work [53].

Nonlinear optical response

The two-photon absorption (TPA) spectrum can be determined from the imaginary component of the third order polarizability of the system [65]; assuming the system is initially in the ground state, the largest contribution to the third order polarizability for two-photon absorption [66] is given by

$$\alpha^{(3)}_{klop}(\omega;\omega,\omega,-\omega) \approx \frac{1}{\epsilon_0\hbar^3}\mathcal{P}_I\sum_{vnm}\frac{\mu^k_{gv}\mu^l_{vn}\mu^o_{nm}\mu^p_{mg}}{(\omega_{vg}-\omega-i\gamma_{vg})(\omega_{ng}-2\omega-i\gamma_{ng})(\omega_{mg}-\omega-i\gamma_{mg})}, \tag{9}$$

where ω is the frequency, $\mathcal{P}_I$ is the permutation operator in the set of distinct frequencies $\{\omega,\omega,-\omega\}$, k,l,o,p are Cartesian components, $\hbar\omega_{vm}$ is the energy difference between states v and m, and γ_{vg} is the frequency broadening associated with the transition $GS \rightarrow v$. The two-photon absorption coefficient measured in experiments is proportional to the imaginary component of the third order susceptibility of the system [67], which can be obtained from the third order polarizability [65]. The predicted strength of the two-photon transition from the ground state to the state Z is given by

$$B_{klop}(GS \rightarrow Z) = \frac{\pi}{2\epsilon_0\hbar^3}\sum_{vm}\frac{\mu^k_{gv}\mu^l_{vZ}\mu^o_{Zm}\mu^p_{mg}}{(\omega_{vg}-\overline{\omega})(\omega_{mg}-\overline{\omega})}, \tag{10}$$

where $\overline{\omega} = \omega_{Zg}/2$. A derivation of $B_{klop}(GS \rightarrow Z)$ is presented in Appendix A.

III. OPTICAL ABSORPTION OF DBT

A. Linear absorption spectrum and spatial profiles of bright transitions

In Fig. 3(a), we plot the oscillator strengths of the bright transitions of DBT assuming the system is initially in the ground state. Recall that the strength of the Coulomb repulsion parameter U was set so the energy of $GS \rightarrow S_1$ is 1.58 eV, in agreement with the experimental value. The radiative linewidth of $GS \rightarrow S_1$ in vacuum [68] is given by

$$\Gamma^{\text{vac}}_{S_1} = \frac{\omega^3_{S_1g}|\boldsymbol{\mu}_{S_1g}|^2}{3\pi\epsilon_0\hbar c^3}, \tag{11}$$

where c is the speed of light, ω_{S_1g} is the frequency difference between the S_1 state and the ground state, and $|\boldsymbol{\mu}_{S_1g}|$ is the magnitude of the matrix element of the dipole moment operator between the ground state and the S_1 state; we find $|\boldsymbol{\mu}_{S_1g}| = 13.1$ D. Due to local field effects, the radiative linewidth of $GS \rightarrow S_1$ is modified when DBT is deposited in an anthracene matrix. There is some controversy as to which is the most appropriate model to describe the local field effects when calculating the radiative linewidth of emitters embedded in a homogeneous medium [69,70]. The real cavity model describes local field effects when the emitters, in this case the DBT molecules, enter the medium as dopants [69,70]. Accounting for local field effects using the real cavity model, the radiative linewidth of the $GS \rightarrow S_1$ transition is

$$\Gamma^{\text{RC}}_{S_1} = n_{\text{eff}}\left(\frac{3n^2_{\text{eff}}}{2n^2_{\text{eff}}+1}\right)^2\Gamma^{\text{vac}}_{S_1}, \tag{12}$$

where n_{eff} is the effective refractive index of the material. Since the concentration of DBT in the anthracene matrix is extremely dilute [23,25], we take n_{eff} to be the refractive index of anthracene. Using Eq. (12), we calculate the radiative linewidth of $GS \rightarrow S_1$ to be 40 MHz; a complete neglect of local field corrections leads to a predicted radiative linewidth of 30 MHz. Measurements of the homogeneously broadened radiative linewidth of the $GS \rightarrow S_1$ transition range from 30 to 40 MHz [3,19,37]. These measurements were carried out at cryogenic temperatures, at which the radiative linewidth is generally assumed to be limited only by the excited state lifetime [3,71]. Given that our calculated radiative linewidth is in the range of reported experimental values, and assuming the experimental value of the radiative linewidth is indeed limited only by the excited state lifetime, then the magnitude of our calculated $GS \rightarrow S_1$ transition dipole moment is also consistent with the experimental values.

In our calculations, the lowest triplet state, T_1, has energy 0.85 eV above the ground state, which is about half the energy of the first singlet excited state above the ground state. The energy of the triplet state is calculated to be greater than the corresponding value calculated by Deperasinska *et al.* [44] by 0.62 eV. Their calculation predicts that the T_1 state is 0.23 eV above the ground state; however, they point out that the method they use to calculate the energies of the excited states exhibits an average deviation of 0.4 eV between the calculated energies

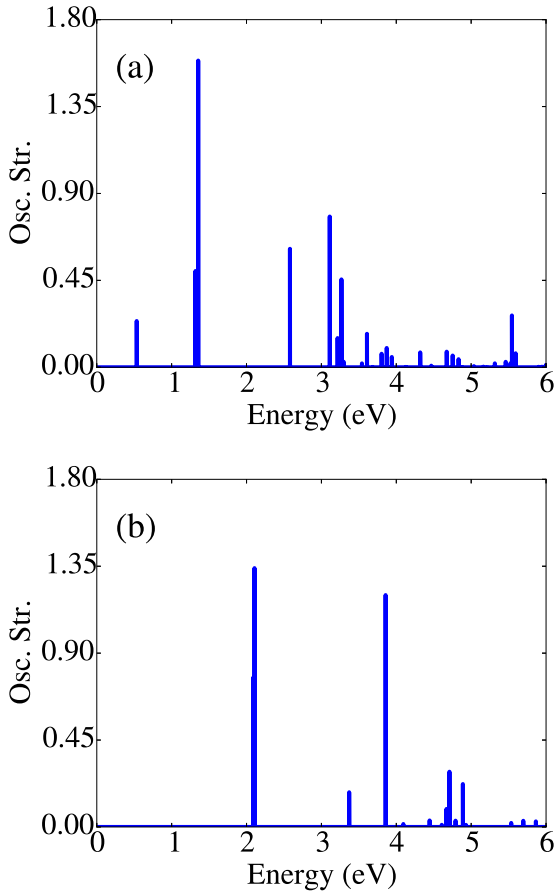

FIG. 4. Absolute oscillator strengths of the bright transitions with (a) the first singlet state S_1 and (b) the first triplet state T_1, as the initial state. Further absorption from the S_1 or T_1 state does not fall within the energy range of the transition from the ground state to the S_1 state.

and the experimental values for small molecules, and gives less accurate results for systems as large as DBT [44,50,51]. The energies of the lowest triplet excited states in the -acene series, which are similar in structure to DBT, are approximately 1 eV above the ground state [46]; in the -acene series, the energy above the ground state of the lowest triplet excited state is approximately half of the energy above the ground state of the lowest singlet excited state, as we find for DBT. The energy of the triplet state in DBT has yet to be experimentally determined. Absorption to the other excited states requires photon energies greater than 3 eV. Our calculations indicate that there are no other absorption peaks close in energy to the absorption peak due to $GS \rightarrow S_1$, and we predict that there are no competing linear optical processes that might reduce the efficacy of the application of this material as a single-photon source. The plot of the energies of the excited states above the ground state, shown in Fig. 3(b), indicates that there are no other excited states that are lower in energy than the S_1 state, except for the T_1 state. Thus from our calculations the only other major relaxation channel is the intersystem crossing to the T_1 state.

To consider the possible significance of sequential absorption from the ground state, we investigate the oscillator strengths of the bright transitions with (a) S_1 and (b) T_1 as the initial state. We plot these oscillator strengths in Fig. 4. It is clear that further absorption from the S_1 state either occurs at photon energies below (less than 0.5 eV) or above (greater than 2 eV) the energy of $GS \rightarrow S_1$. If the excitation decays to the triplet state, due to intersystem crossing for example, any further absorption from the triplet state occurs at photon energies that are much higher (greater than 2 eV) than the energy of $GS \rightarrow S_1$. Our calculations indicate that there is no further absorption from the S_1 or T_1 state for the energy range of interest of the application of DBT as a single-photon source.

The sums of the oscillator strengths in Figs. 3(a), 4(a), and 4(b) are respectively 5.35, 5.49, and 4.28, and the number of electrons included in the calculation is 10; thus, as expected, these transitions do not exhaust the f-sum rule [72].

Reasonable variations of the Hubbard U and the screening parameter ϵ do not affect our conclusions: the energies above the ground state of the electronic states shift as U and ϵ are adjusted; however, there are still no linear absorption peaks near the energy of $GS \rightarrow S_1$, and there is no further absorption from the S_1 state and the T_1 state at the energy of $GS \rightarrow S_1$. Details of how the calculated linear optical properties of DBT change as U and ϵ are adjusted are outlined in Appendix B.

The linear optical properties of the buckled structure of the DBT molecule are similar to those of the flat structure: There are small shifts in the energies of the electronic states and differences in oscillator strengths for the bright transitions;

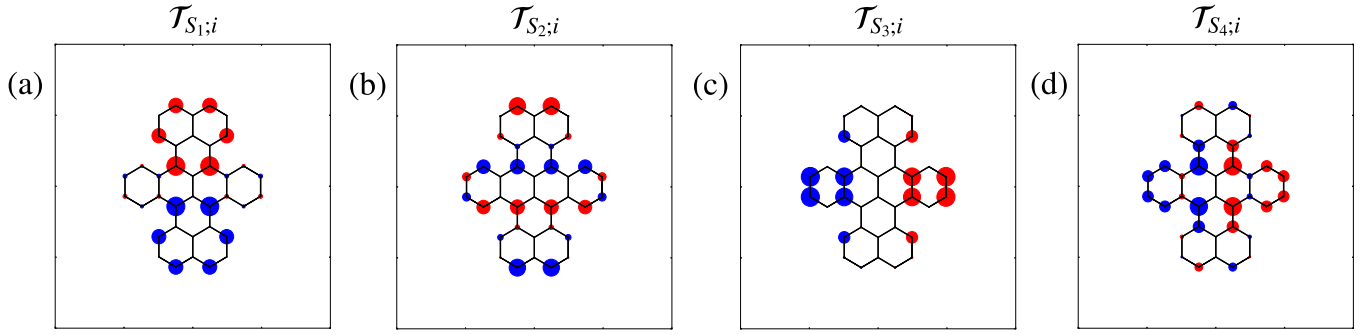

FIG. 5. Plots of (a) $\mathcal{T}_{S_1;i}$, (b) $\mathcal{T}_{S_2;i}$, (c) $\mathcal{T}_{S_3;i}$, and (d) $\mathcal{T}_{S_4;i}$. We place a circle at the location of each site i; the area of each circle indicates the magnitude of $\mathcal{T}_{Y;i}$ and the color indicates whether it is positive (red) or negative (blue). The convention used for labeling these states follows energetic order, i.e., S_1 is the lowest energy state, S_2 is the second lowest energy state, and so on. The transitions that are polarized along the $\hat{\mathbf{y}}$ axis have electron concentration extended throughout the system, while those polarized along the $\hat{\mathbf{x}}$ axis have electron concentration primarily in the middle of the system; the axes are shown in Fig. 2.

TABLE I. Lowest three two-photon transitions of DBT, their associated fundamental photon energies $\hbar\omega$, the associated integrated third order polarizability strengths, and the component of the third order polarizability tensor that exhibit the peaks.

Transition	$\hbar\omega$ (eV)	Strength (μm^5/V^{2}s)	Component
$GS \rightarrow 2LH$	1.06	0.599	$yyyy$
$GS \rightarrow S_{D_1}$	1.45	8.08	$yxxy$
$GS \rightarrow S_{D_2}$	1.47	33.8	$yyyy$

however, these discrepancies are not significant. The details of the linear optical properties of the buckled structure of DBT are also presented in Appendix B.

Finally, we turn to the spatial profiles of the bright transitions from the ground state of DBT. We calculate $\mathcal{T}_{Y;i}$ for the first four bright excited states, and plot them in Fig. 5. The molecular axes are shown in Fig. 2. The transition dipole moments associated with the first two optical transitions, $GS \rightarrow S_1$ and $GS \rightarrow S_2$, are polarized along the $\hat{\mathbf{y}}$ axis. The spatial profile of $GS \rightarrow S_1$ has electron density extended across the entire system and leads to a very large transition dipole moment. The spatial profile of $GS \rightarrow S_2$ has electron concentration extended across the entire system, much like $\mathcal{T}_{S_1;i}$, but has a weaker transition dipole moment. The transition dipole moments associated with the next two optical transitions, $GS \rightarrow S_3$ and $GS \rightarrow S_4$, are polarized along the $\hat{\mathbf{x}}$ axis. The spatial profile of $GS \rightarrow S_3$ has electron density primarily on the four rings in the middle of the system, and it has very little concentration on the top and bottom rings; it leads to a very large transition dipole moment. The spatial profile of $GS \rightarrow S_4$ has significant electron concentration in the middle of the system, and it has negligible electron concentration in the top and bottom rings of the system; it leads to a weaker transition dipole moment. For transitions with dipole moment polarized along the $\hat{\mathbf{y}}$ axis, the electron density is extended across the entire system, but for transitions with dipole moment polarized along the $\hat{\mathbf{x}}$ axis, the electron density is concentrated at the center of the system.

B. Two-photon absorption spectrum

For the two-photon transitions of interest, we compute their associated fundamental photon energies, two-photon transition strengths, and the components of the third order polarizability tensor that exhibit the peaks. In Table I we show the values of these quantities. The lowest energy TPA is due to $GS \rightarrow 2LH$, and arises from Im $(\alpha^{(3)}_{yyyy})$; the $2LH$ state is composed mainly of HF double excitations. The next two TPA peaks are due to $GS \rightarrow S_{D_1}$ [from Im $(\alpha^{(3)}_{yxxy})$] and $GS \rightarrow S_{D_2}$ [from Im $(\alpha^{(3)}_{yyyy})$]; the S_{D_1} state and the S_{D_2} state are composed mainly of HF single excitations. The two-photon transitions $GS \rightarrow S_{D_1}$ and $GS \rightarrow S_{D_2}$ occur when the fundamental photon energy $\hbar\omega$ is close to the energy of the single-photon transition $GS \rightarrow S_1$. The calculated strength of the TPA in DBT is in line with the TPA calculated in other conjugated organic systems [46,63].

From the values of the calculated energies and the calculated absorption strengths, we argue that for the single-photon source application of DBT, the TPA should not compete with $GS \rightarrow S_1$ in any meaningful way.

First we consider that a continuous wave (cw) laser is used to pump $GS \rightarrow S_1$ [25]. Since the spectral width of cw lasers is usually less than 0.01 meV, the spectrum of a cw laser centered at $\omega_{S_1 g}$ will not contain the frequency components required to excite either S_{D_1} or S_{D_2}.

Second we consider the excitation by optical pulses, as done in a number of experiments [3,18,73]. For example, Toninelli *et al.* [18] used a Ti:sapphire laser with a spectrum centered near $\omega_{S_1 g}$ and a pulse duration of 120 fs to excite $GS \rightarrow S_1$. The spectrum of these pulses has the necessary frequency components to excite the two-photon active transitions near $GS \rightarrow S_1$. To investigate the possible consequences of TPA, we use a perturbative treatment [74] to calculate the one-photon absorption to the S_1 state and the two-photon absorption to the S_{D_2} state. This approach is a generalization of Eq. (23) in Ref. [53], and Eq. (9) respectively for pulsed pumping. We model the laser pulse as an unchirped Gaussian centered at $\omega_{S_1 g}$ with an intensity full width at half maximum (FWHM) of τ. Upon excitation of DBT, the population ρ_{S_1} of the S_1 state at times after the pulse is

$$\rho_{S_1} = \left(\frac{\pi |\boldsymbol{\mu}_{S_1 g}|^2}{(4 \ln 2) n_{\text{eff}} \epsilon_0 c \hbar^2} \right) \tau^2 I_0, \tag{13}$$

where I_0 is the peak intensity; I_0 can be written in terms of the pulse energy as

$$I_0 = \frac{2\sqrt{\ln 2}}{\sqrt{\pi}\tau} \frac{Q_{\text{pulse}}}{A_{\text{pulse}}}, \tag{14}$$

where Q_{pulse} is the pulse energy and A_{pulse} is the area of the laser spot. The population $\rho_{S_{D_2}}$ of the S_{D_2} state at such times is given by

$$\frac{\rho_{S_{D_2}}}{\rho_{S_1}} = \left(\frac{|\boldsymbol{\mu}_{S_{D_2} S_1}|^2 |\mathcal{F}|^2}{(16 \ln 2) \pi n_{\text{eff}} \epsilon_0 c \hbar^2} \right) \tau^2 I_0. \tag{15}$$

Here $|\boldsymbol{\mu}_{S_{D_2} S_1}|$ is the magnitude of the matrix element of the dipole moment operator between the S_1 state and the S_{D_2} state; from our calculations $|\boldsymbol{\mu}_{S_{D_2} S_1}| = 17.6$ D. The term $\mathcal{F}$ is

$$\mathcal{F} = \int_{-\infty}^{\infty} \frac{\exp\left(-\frac{\tau^2}{4 \ln 2} (\omega - \omega_{S_1 g})^2 \right) \exp\left(-\frac{\tau^2}{4 \ln 2} (\omega_{S_{D_2} g} - \omega - \omega_{S_1 g})^2 \right)}{(\omega_{S_1 g} - \omega - i(\Gamma_{S_1}/2))} d\omega, \tag{16}$$

where $\omega_{S_{D_2} g}$ is the frequency difference between the S_{D_2} state and the ground state and Γ_{S_1} is the linewidth of $GS \rightarrow S_1$ given by (12). For $\tau = 120$ fs, $|\mathcal{F}|^2 \approx 5.58 \times 10^{-4}$.

In a previous experimental study of DBT [18], pulsed lasers with an average power of 3 W, a repetition rate of 76 MHz, and resulting peak intensities ranging from 500 to 4000 kW/cm^2 were used to excite $GS \rightarrow S_1$; for these peak intensities, we predict that the ratio of the populations of the S_{D_2} state and the S_1 state (15) is on the order of 10^{-7}. At a peak intensity of 30 MW/cm^2 (corresponding to a pulse energy of 0.32 nJ

and assuming a circular laser spot with a radius of 50 μm), our perturbative assumption (i.e., the excitation by the laser pulse is weak) breaks down, and the predicted population of the S_1 state is large ($\rho_{S_1} \approx 0.2$). For this peak intensity of the pulse, the ratio between the populations of the S_{D_2} state and the S_1 state (15) is on the order of 10^{-6}. This indicates that even for intensities strong enough to significantly populate the S_1 state, the population of the S_{D_2} state will be minuscule relative to the population of the S_1 state.

Reasonable variations of U and ϵ can result in the difference between the energy of $GS \rightarrow S_1$, and the fundamental photon energy involved in the two-photon transition $GS \rightarrow S_{D_2}$, being as low as 0.04 eV. Even for such a small difference in energy, our perturbative calculation indicates that, at a peak intensity of 30 MW/cm^2, the ratio of the population of the S_{D_2} state and the population of the S_1 state is on the order of 10^{-2}. Thus our assertion that TPA will not impact the single-photon source application of DBT still holds. As with the linear optical properties, the nonlinear optical properties of the buckled structure of the DBT molecule are similar to those of the flat structure. Details of how the calculated nonlinear optical properties of DBT change as parameters are varied are outlined in Appendix B.

IV. CONCLUSION

We applied a method developed for the description of the electronic and optical properties of graphene flakes to study the optical properties of dibenzoterrylene (DBT), a candidate material for single-photon source applications. We set the Hubbard U parameter of our calculation such that the lowest energy singlet excited state, labeled S_1, is 1.58 eV above the ground state energy, in agreement with the experimental value. Our calculated radiative linewidth for the transition from the ground state to the S_1 state (denoted $GS \rightarrow S_1$) agrees with the experimental value as well. Assuming the experimental measurement of the radiative linewidth is limited only by the excited state lifetime, then our calculated value of the $GS \rightarrow S_1$ transition dipole moment is consistent with its experimental value.

For DBT to be a good single-photon source, there should be no other optical processes that compete with the transition from the ground state to the first singlet excited state: There should be no other linear absorption peaks near the peak due to $GS \rightarrow S_1$; further absorption from the S_1 state should not occur at photon energies near the energy of $GS \rightarrow S_1$; intersystem crossing to the first triplet state, labeled T_1, should not be significant; and further absorption from the T_1 state also should not occur at photon energies near the energy of $GS \rightarrow S_1$.

We calculated the oscillator strengths of the bright transitions of DBT up to 6.0 eV, which should be useful for testing the model against future experiments; excitations from the sp^2 states, not included in this model, are not expected to be in this energy range. Our calculations predict that there are no other competing linear absorption features near the energy of $GS \rightarrow S_1$. We also calculated the further absorption from the S_1 state; our calculations indicate that there is no further absorption from the S_1 state for the energy range of interest in the application of DBT as a single-photon source. We characterized the charge distributions involved in the bright transitions of DBT, and we showed that the spatial profiles of transitions which have transition dipole moments that are polarized along the $\hat{\mathbf{y}}$ axis have electron concentration extended over the entire system, while the spatial profiles of transitions which have transition dipole moments polarized along the $\hat{\mathbf{x}}$ axis have electron concentration primarily in the center of the system.

Our calculations indicate that the T_1 state has energy 0.85 eV above the ground state; in our calculation, the energy above the ground state of the T_1 state is approximately half the energy above the ground state of the S_1 state. Such a large difference in energy between the S_1 state and the T_1 state indicates that the intersystem crossing rate is small in DBT [41,42]. We calculated the further absorption from the T_1 state; our calculations indicate that there is no further absorption from the T_1 state for the energy range of interest in the application of DBT as a single-photon source.

We also calculated the two-photon absorption (TPA) of DBT. An understanding of the nonlinear optical properties of DBT is important for general optical applications, and also for the specific application of DBT as a single-photon source since it reveals whether there are any competing nonlinear optical processes against the optical transition that generate the desired photons. The TPA spectrum showed that in the low-photon energy regime, three states are two-photon active: a state composed primarily of HF double excitations and two states composed mainly of HF single excitations. The strong two-photon absorption occurs at fundamental photon energies near the energy of $GS \rightarrow S_1$. If narrow frequency laser pulses (with a temporal full width at half maximum greater than 120 fs) and weak peak intensities (on the order of 1000 kW/cm^2) or continuous wave lasers are used to excite $GS \rightarrow S_1$, then the strong TPA that occurs at photon energies near the energy of $GS \rightarrow S_1$ should not hinder the single-photon source application of DBT.

Therefore, our calculations indicate that DBT is a good candidate for a single-photon source, as there are no other competing absorption features near the energy of the transition from the ground state to the S_1 state. Our conclusions are robust to reasonable variations of the Hubbard U and the screening parameter ϵ. The calculations we have performed have also elucidated qualitative features of the higher energy absorption spectrum of DBT, and we expect that these qualitative features will be of interest for considering the use of DBT for other optical applications besides as single-photon sources.

APPENDIX A: INTEGRATED THIRD ORDER POLARIZABILITY

In this appendix, we derive an expression for the integrated third polarizability. The largest contribution to the third order polarizability [66] is given by

$$\alpha^{(3)}_{\mathrm{klop}}(\omega;\omega,\omega,-\omega) \approx \frac{1}{\epsilon_0\hbar^3}\sum_{\mathrm{vnm}}\frac{\mu^k_{gv}\mu^l_{vn}\mu^o_{nm}\mu^p_{mg}}{(\omega_{vg}-\omega-i\gamma_{vg})(\omega_{ng}-2\omega-i\gamma_{ng})(\omega_{mg}-\omega-i\gamma_{mg})} \tag{A1}$$

TABLE II. Predicted energy above the ground state of the S_1 state, the $\Gamma_{S_1}^{\mathrm{NLF}}$ quantity, and the $\Gamma_{S_1}^{\mathrm{RC}}$ quantity for various values of U. The term $\Gamma_{S_1}^{\mathrm{NLF}}$ is the calculated radiative linewidth of $GS \rightarrow S_1$ when neglecting local field effects; $\Gamma_{S_1}^{\mathrm{NLF}}$ is given by $\Gamma_{S_1}^{\mathrm{NLF}} = n_{\mathrm{eff}}\Gamma_{S_1}^{\mathrm{vac}}$. For these calculations, we set $t_{ij} = 2.66$ eV for the π conjugated bonds, $t_{ij} = 2.22$ eV for the single bonds, and $\epsilon = 5$. The experimental value for the energy above the ground state of the S_1 state is 1.58 eV and the experimental value of the radiative linewidth of $GS \rightarrow S_1$ ranges from 30 to 40 MHz [3,19,37].

U (eV)	E_{S_1} (eV)	$\Gamma_{S_1}^{\mathrm{NLF}}$ (MHz)	$\Gamma_{S_1}^{\mathrm{RC}}$ (MHz)
5.08	1.48	20	40
5.48	1.53	30	40
5.88	1.58	30	40
6.29	1.63	30	50
6.69	1.69	30	50

near the $\omega_{ng} \approx 2\omega$ resonance. At such frequencies, we are far away from the ω_{vg} and the ω_{ng} resonances and, therefore, we can neglect the linewidths γ_{vg} and γ_{mg}; the third order polarizability (A1) can then be further approximated as

$$\alpha_{\mathrm{klop}}^{(3)} \approx \frac{1}{\epsilon_0\hbar^3}\sum_{\mathrm{vnm}}\frac{\mu_{gv}^k\mu_{vn}^l\mu_{nm}^o\mu_{mg}^p}{(\omega_{vg}-\overline{\omega})(\omega_{mg}-\overline{\omega})}\frac{1}{(\omega_{ng}-2\omega-i\gamma_{ng})}, \tag{A2}$$

where $\overline{\omega} = \omega_{ng}/2$. The imaginary component of (A2) is given by

$$\mathrm{Im}\left(\alpha_{\mathrm{klop}}^{(3)}\right) \approx \frac{1}{\epsilon_0\hbar^3}\sum_{\mathrm{vnm}}\frac{\mu_{gv}^k\mu_{vn}^l\mu_{nm}^o\mu_{mg}^p}{(\omega_{vg}-\overline{\omega})(\omega_{mg}-\overline{\omega})}\frac{\gamma_{ng}}{(\omega_{ng}-2\omega)^2+\gamma_{ng}^2}. \tag{A3}$$

We then integrate (A3) over all frequencies ω; this is done so that the resulting expression is independent of the linewidth γ_{ng}. Integrating (A3) over all frequencies, we obtain

$$\int_{-\infty}^{\infty}\mathrm{Im}\left(\alpha_{\mathrm{klop}}^{(3)}\right)d\omega \approx \frac{\pi}{2\epsilon_0\hbar^3}\sum_{\mathrm{vnm}}\frac{\mu_{gv}^k\mu_{vn}^l\mu_{nm}^o\mu_{mg}^p}{(\omega_{vg}-\overline{\omega})(\omega_{mg}-\overline{\omega})}, \tag{A4}$$

where we have used $\int_{-\infty}^{\infty}1/((2x-x_0)^2+\gamma_{ng}^2)dx = \pi/2\gamma_{ng}$. The expression (A4) is the integrated third order polarizability, which is independent of the frequency broadening γ_{ng}. Therefore, the strength of the two photon transition $GS \rightarrow Z$ is given by

$$B_{\mathrm{klop}}(GS \rightarrow Z) = \frac{\pi}{2\epsilon_0\hbar^3}\sum_{vm}\frac{\mu_{gv}^k\mu_{vZ}^l\mu_{Zm}^o\mu_{mg}^p}{(\omega_{vg}-\overline{\omega})(\omega_{mg}-\overline{\omega})}, \tag{A5}$$

which is Eq. (10).

APPENDIX B: PARAMETER SENSITIVITY

In this appendix, we discuss how varying the Hubbard U, the screening parameter ϵ, and the structure of the molecule affects the calculated linear and nonlinear optical properties of DBT.

1. Effects of the variation of the Hubbard U on the optical properties of DBT

We first examine how variations of the Hubbard U affect the calculated optical properties of DBT. We change the Hubbard U while keeping the hopping parameters and the screening parameter ϵ constant; for these calculations, we set $t_{ij} = 2.66$ eV for the π conjugated bonds, $t_{ij} = 2.22$ eV for the single bonds, and $\epsilon = 5$. We restrict ourselves to values of U such that the maximum deviation between the predicted and the experimental S_1 transition energy equals 0.1 eV.

We tabulate the energy above the ground state of the S_1 state and the radiative linewidth of $GS \rightarrow S_1$, a measure of the accuracy of the calculation, for several values of U in Table II. For values of $U > 6.69$ eV and $U < 5.08$ eV, the deviation between the predicted S_1 transition energy and the experimentally measured quantity is greater than 0.1 eV, and the calculated radiative linewidth of $GS \rightarrow S_1$ is inconsistent with the experimentally determined range of values. The S_1 transition energy increases as U increases.

Next, we investigate the TPA as we vary U. We tabulate the energy of the dark state S_{D_2} and the difference between the energy of $GS \rightarrow S_1$ and the fundamental photon energy involved in the two-photon transition $GS \rightarrow S_{D_2}$, which we denote as $\Delta E = E_{S_1} - (E_{S_{D_2}}/2)$, for several values of U in Table III. As we vary U, ΔE becomes smallest ($\Delta E = 0.04$ eV) at $U = 5.08$ eV; even at this small energy difference, a cw laser centered at $\omega_{S_1 g}$ will not be able to excite the S_{D_2} state as the spectral width of a typical cw laser is usually less than 0.01 meV. Next, consider the excitation of DBT by optical

TABLE III. Energy above the ground state of the dark state S_{D_2}, the difference between the energy of $GS \rightarrow S_1$ and the fundamental photon energy involved in the two-photon transition $GS \rightarrow S_{D_2}$ [$\Delta E = E_{S_1} - (E_{S_{D_2}}/2)$], and the population of the S_{D_2} state ($\rho_{S_{D_2}}$) relative to the population of the S_1 state (ρ_{S_1}) upon excitation by an optical pulse at various intensities, for several values of U. The laser pulse is modeled as an unchirped Gaussian centered at $\omega_{S_1 g}$ with an intensity full width at half maximum of $\tau = 120$ fs. In typical experimental studies of DBT, a peak intensity of $I_0 = 4000$ kW/cm^2 is used to irradiate the system; at a peak intensity of $I_0 = 30$ MW/cm^2 our perturbative approach begins to break down ($\rho_{S_1} \approx 0.2$).

U (eV)	E_{S_1} (eV)	$E_{S_{D_2}}$ (eV)	ΔE (eV)	$\rho_{S_{D_2}}/\rho_{S_1}$ at $I_0 = 4000$ kW/cm^2	$\rho_{S_{D_2}}/\rho_{S_1}$ at $I_0 = 30$ MW/cm^2
5.08	1.48	2.88	0.04	10^{-3}	10^{-2}
5.48	1.53	2.91	0.07	10^{-4}	10^{-3}
5.88	1.58	2.94	0.11	10^{-7}	10^{-6}
6.29	1.63	2.96	0.15	10^{-10}	10^{-9}
6.69	1.69	2.99	0.20	10^{-14}	10^{-13}

TABLE IV. Predicted energy above the ground state of the S_1 state, the $\Gamma_{S_1}^{\mathrm{NLF}}$ quantity, and the $\Gamma_{S_1}^{\mathrm{RC}}$ quantity for various values of ϵ. The term $\Gamma_{S_1}^{\mathrm{NLF}}$ is the calculated radiative linewidth of $GS \rightarrow S_1$ when neglecting local field effects; $\Gamma_{S_1}^{\mathrm{NLF}}$ is given by $\Gamma_{S_1}^{\mathrm{NLF}} = n_{\mathrm{eff}}\Gamma_{S_1}^{\mathrm{vac}}$. For these calculations, we set $t_{ij} = 2.66$ eV for the π conjugated bonds, $t_{ij} = 2.22$ eV for the single bonds, and $U = 5.88$ eV. The experimental value for the energy above the ground state of the S_1 state is 1.58 eV and the experimental value of the radiative linewidth of $GS \rightarrow S_1$ ranges from 30 to 40 MHz [3,19,37].

ϵ	E_{S_1} (eV)	$\Gamma_{S_1}^{\mathrm{NLF}}$ (MHz)	$\Gamma_{S_1}^{\mathrm{RC}}$ (MHz)
2.5	1.67	30	50
5	1.58	30	40
10	1.52	30	40

pulses. We model the laser pulse as an unchirped Gaussian centered at $\omega_{S_1 g}$ with a full width half maximum of $\tau = 120$ fs. We find that upon the excitation of DBT by an optical pulse at a peak intensity of $I_0 = 4000\,\mathrm{kW/cm^2}$, even for $\Delta E = 0.04$ eV, the population of the S_{D_2} state ($\rho_{S_{D_2}}$) is negligible compared to the population of the S_1 state (ρ_{S_1}); even at intensities where our perturbative treatment breaks down ($I_0 = 30\ \mathrm{MW/cm^2}$), the ratio of $\rho_{S_{D_2}}$ and ρ_{S_1} is on the order of 10^{-2}.

2. Effects of the variation of the screening parameter ϵ on the optical properties of DBT

In this section, we discuss how varying the screening parameter ϵ affects the calculated optical properties of DBT. We change the screening parameter ϵ while keeping the hopping parameters and the Hubbard U constant; for these calculations, we set $t_{ij} = 2.66$ eV for the π conjugated bonds, $t_{ij} = 2.22$ eV for the single bonds, and $U = 5.88$ eV. We restrict ourselves to values of ϵ such that the maximum deviation between the predicted and the experimental S_1 transition energy equals 0.1 eV.

We tabulate the energy above the ground state of the S_1 state and the radiative linewidth of $GS \rightarrow S_1$, a measure of the accuracy of the calculation, for several values of ϵ in Table IV. For values of $\epsilon < 2.5$, the deviation between the predicted S_1 transition energy and the experimentally measured quantity is greater than 0.1 eV and the calculated radiative linewidth of $GS \rightarrow S_1$ is inconsistent with the experimentally determined range of values. The S_1 transition energy decreases as ϵ increases.

Finally, we investigate the TPA as we vary ϵ. We tabulate the energy of the dark state S_{D_2} and the difference between the energy of $GS \rightarrow S_1$ and the fundamental photon energy involved in the two-photon transition $GS \rightarrow S_{D_2}$, which we denote as $\Delta E = E_{S_1} - (E_{S_{D_2}}/2)$, for several values of ϵ in Table V. As we vary ϵ, ΔE becomes smallest ($\Delta E = 0.04$ eV) at $\epsilon = 2.5$; even at this small energy difference, a cw laser centered at $\omega_{S_1 g}$ will not be able to excite the S_{D_2} state as the spectral width of a typical cw laser is usually less than 0.01 meV. Next, consider the excitation of DBT by optical pulses. We model the laser pulse as an unchirped Gaussian centered at $\omega_{S_1 g}$ with a full width at half maximum of $\tau = 120$ fs. We find that upon the excitation of DBT by an optical pulse at a peak intensity of $I_0 = 4000\,\mathrm{kW/cm^2}$, even for $\Delta E = 0.04$ eV, the population of the S_{D_2} state ($\rho_{S_{D_2}}$) is negligible compared to the population of the S_1 state (ρ_{S_1}); even at intensities where our perturbative treatment breaks down ($I_0 = 30\ \mathrm{MW/cm^2}$), the ratio of $\rho_{S_{D_2}}$ and ρ_{S_1} is on the order of 10^{-2}.

3. One-photon and two-photon absorption spectra of the optimized structure of DBT

Finally, we present the one-photon and the two-photon absorption spectra for the optimized structure of DBT (which we refer to as the buckled structure). We acquired the optimized structure for DBT from the PubChem archive [40].

In our model, the extended Coulomb interaction parameters V_{ij} depend on the positions of the carbon atoms; any change in distance between the sites changes the extended Coulomb interaction parameters V_{ij}.

We plot the oscillator strengths of the bright transitions and the energies of the excited states above the ground state of DBT for both the "flat" and the "buckled" structure in Fig. 6. There are small shifts in the energies of the electronic excited states and slight differences in oscillator strengths of the bright transitions for the buckled structure, but they are not significant. The buckled structure exhibits several new absorption peaks; however, the energies of these new absorption peaks are not close in energy to the absorption peak due to $GS \rightarrow S_1$, and their existence does not affect our conclusions. Our calculated radiative linewidth of the $GS \rightarrow S_1$ transition for the buckled structure ranges from 30 to 40 MHz, in excellent agreement with the experimentally measured values.

We also plot the oscillator strengths of the bright transitions assuming (a) the S_1 state as the initial state and (b) the T_1 state

TABLE V. Energy above the ground state of the dark state S_{D_2}, the difference between the energy of $GS \rightarrow S_1$ and the fundamental photon energy involved in the two-photon transition $GS \rightarrow S_{D_2}$ [$\Delta E = E_{S_1} - (E_{S_{D_2}}/2)$], and the population of the S_{D_2} state ($\rho_{S_{D_2}}$) relative to the population of the S_1 state (ρ_{S_1}) upon excitation by an optical pulse at various intensities, for several values of ϵ. The laser pulse is modeled as an unchirped Gaussian centered at $\omega_{S_1 g}$ with an intensity full width at half maximum of $\tau = 120$ fs. In typical experimental studies of DBT, a peak intensity of $I_0 = 4000\,\mathrm{kW/cm^2}$ is used to irradiate the system; at a peak intensity of $I_0 = 30\ \mathrm{MW/cm^2}$ our perturbative approach begins to break down ($\rho_{S_1} \approx 0.2$).

ϵ	E_{S_1} (eV)	$E_{S_{D_2}}$ (eV)	ΔE (eV)	$\rho_{S_{D_2}}/\rho_{S_1}$ at $I_0 = 4000\,\mathrm{kW/cm^2}$	$\rho_{S_{D_2}}/\rho_{S_1}$ at $I_0 = 30\ \mathrm{MW/cm^2}$
2.5	1.67	3.26	0.04	10^{-3}	10^{-2}
5	1.58	2.94	0.11	10^{-7}	10^{-6}
10	1.52	2.74	0.15	10^{-9}	10^{-8}

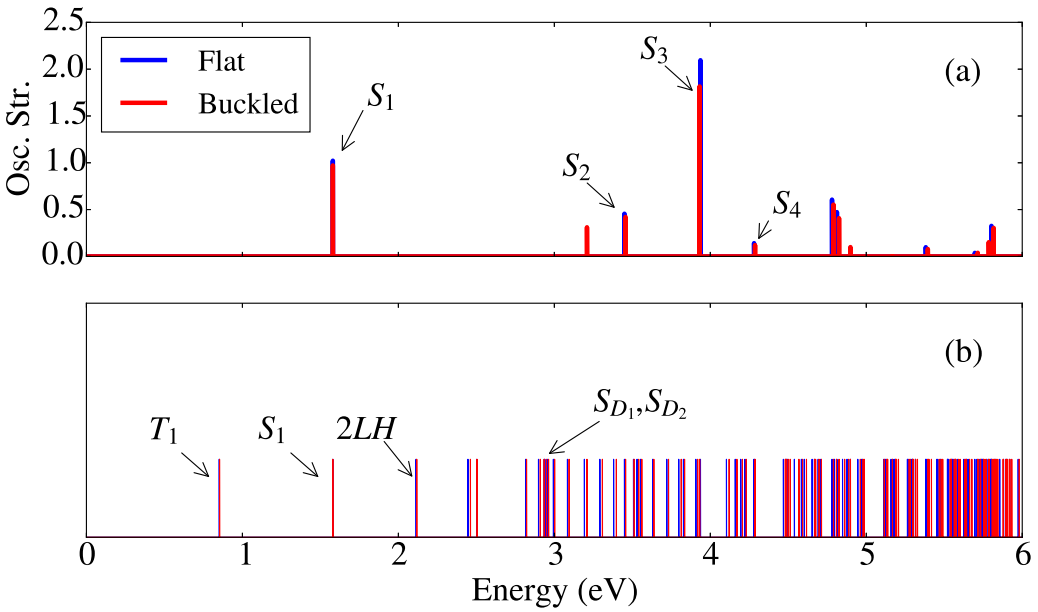

FIG. 6. (a) Plot of the oscillator strengths of the bright transitions and (b) the energies of the excited states above the ground state of DBT for both the flat and the buckled structure of DBT.

as the initial state for both the flat and the buckled structure in Fig. 7. Again, there are small shifts in the energies of the electronic excited states and slight differences in the oscillator strengths of the bright transitions for the buckled structure, but they are not significant. The buckled structure exhibits several new absorption peaks; however, these peaks are not close in energy to the absorption peak due to $GS \rightarrow S_1$ and their existence does not affect our conclusions.

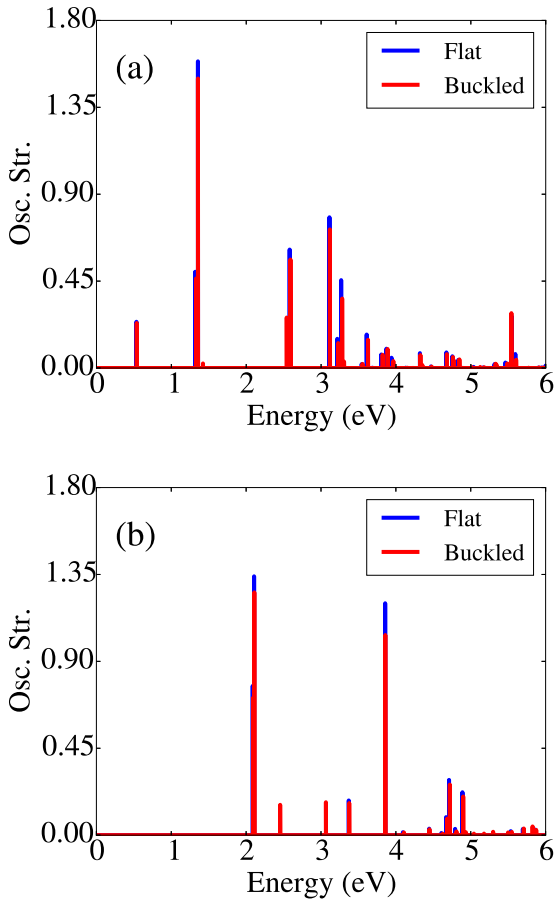

FIG. 7. Oscillator strengths of the bright transitions with (a) the first singlet excited state S_1 and (b) the first triplet excited state T_1, as the initial state for both the flat and the buckled structure.

In Table VI, we show the fundamental photon energy, two-photon transition strength, and the component of the third order polarizability tensor that exhibit the peaks of the four lowest two-photon transitions for the buckled structure. The three lowest energy two-photon transitions do not differ significantly from the results for the flat structure (see Table I). The transition $GS \rightarrow S_{D_3}$ only becomes two-photon active for the buckled structure. The S_{D_3} state has a higher energy above the ground state than both the S_{D_1} and the S_{D_2} states; S_{D_3} is composed primarily of HF single excitations. While the fundamental photon energy involved in the two-photon transition $GS \rightarrow S_{D_3}$ is close to the energy of $GS \rightarrow S_1$, it will not affect the single-photon source application of DBT as the two-photon absorption strength of $GS \rightarrow S_{D_3}$ is extremely weak.

TABLE VI. Lowest four two-photon transitions of the buckled structure of DBT, their associated fundamental photon energies $\hbar\omega$, the associated integrated third order polarizability strengths, and the component of the third order polarizability tensor that exhibits the peaks.

Transition	$\hbar\omega$ (eV)	Strength (μm^5/V^{2}s)	Component
$GS \rightarrow 2LH$	1.06	0.553	$yyyy$
$GS \rightarrow S_{D_1}$	1.45	7.73	$yxxy$
$GS \rightarrow S_{D_2}$	1.47	30.4	$yyyy$
$GS \rightarrow S_{D_3}$	1.50	0.923	$yzzy$

[1] M. D. Eisaman, J. Fan, A. Migdall, and S. V. Polyakov, Rev. Sci. Instrum. **82**, 071101 (2011).

[2] M. Schiavon, G. Vallone, F. Ticozzi, and P. Villoresi, Phys. Rev. A **93**, 012331 (2016).

[3] J.-B. Trebbia, H. Ruf, P. Tamarat, and B. Lounnis, Opt. Express **17**, 23986 (2009).

[4] B. Lounis and M. Orrit, Rep. Prog. Phys. **68**, 1129 (2005).

[5] J. L. O'Brien, Science **318**, 1567 (2007).

[6] C. Kurtsiefer, S. Mayer, P. Zarda, and H. Weinfurter, Phys. Rev. Lett. **85**, 290 (2000).

[7] I. Aharonovich, A. D. Greentree, and S. Prawer, Nat. Photon. **5**, 397 (2011).

[8] M. Müller, H. Vural, C. Schneider, A. Rastelli, O. G. Schmidt, S. Höfling, and P. Michler, Phys. Rev. Lett. **118**, 257402 (2017).

[9] S. Buckley, K. Rivoire, and J. Vučković, Rep. Prog. Phys. **75**, 126503 (2012).

[10] P. Senellart, G. Solomon, and A. White, Nat. Nanotechnol. **12**, 1026 (2017).

[11] D. C. Unitt, A. J. Bennett, P. Atkinson, K. Cooper, P. See, D. Gevaux, M. B. Ward, R. M. Stevenson, D. A. Ritchie, and A. J. Shields, J. Opt. B **7**, S129 (2005).

[12] C. Wang, C. Kurtsiefer, H. Weinfurter, and B. Burchard, J. Phys. B **39**, 37 (2006).

[13] I. A. Khramtsov, M. Agio, and D. Y. Fedyanin, Phys. Rev. Appl. **8**, 024031 (2017).

[14] L. Marseglia, K. Saha, A. Ajoy, T. Schröder, D. Englund, F. Jelezko, R. Walsworth, J. L. Pacheco, D. L. Perry, E. S. Bielejec, and P. Cappellaro, Opt. Express **26**, 80 (2018).

[15] D. B. Higginbottom, L. Slodička, G. Araneda, L. Lachman, R. Filip, M. Hennrich, and R. Blatt, New J. Phys. **18**, 093038 (2016).

[16] M. Hijlkema, B. Weber, H. P. Specht, S. C. Webster, A. Kuhn, and G. Rempe, Nat. Phys. **3**, 253 (2007).

[17] M. Keller, B. Lange, K. Hayasaka, W. Lange, and H. Walther, Nature (London) **431**, 1075 (2004).

[18] C. Toninelli, K. Early, J. Bremi, A. Renn, S. Götzinger, and V. Sandoghdar, Opt. Express **18**, 6577 (2010).

[19] A. A. L. Nicolet, P. Bordat, C. Hofmann, M. A. Kol'chenko, B. Kozankiewicz, R. Brown, and M. Orrit, Chem. Phys. Chem. **8**, 1929 (2007).

[20] A.-M. Boiron, F. Jelezko, Y. Durand, B. Lounis, and M. Orrit, Mol. Cryst. Liq. Cryst. **291**, 41 (1996).

[21] S. Faez, N. R. Verhart, M. Markoulides, F. Buda, A. Gourdon, and M. Orrit, Faraday Discuss. **184**, 251 (2015).

[22] Y. Li, Z. Jia, S. Xiao, H. Liu, and Y. Li, Nat. Commun. **7**, 11637 (2016).

[23] K. D. Major, Y.-H. Lien, C. Polisseni, S. Grandi, K. W. Kho, A. S. Clark, and E. A. Hinds, Rev. Sci. Instrum. **86**, 083106 (2015).

[24] P. E. Lombardi, A. P. Ovvyan, S. Pazzagli, G. Mazzamuto, G. Kewes, O. Neitzke, N. Gruhler, O. Benson, W. H. P. Pernice, F. S. Cataliotti, and C. Toninelli, ACS Photon. **5**, 126 (2018).

[25] C. Polisseni, K. D. Major, S. Boissier, S. Grandi, A. S. Clark, and E. A. Hinds, Opt. Express **24**, 5615 (2016).

[26] T. Farrow, R. A. Taylor, and V. Vedral, Faraday Discuss. **184**, 183 (2014).

[27] Y. Tian, P. Navarro, and M. Orrit, Phys. Rev. Lett. **113**, 135505 (2014).

[28] G. Mazzamuto, A. Tabani, S. Pazzagli, S. Rizvi, A. Reserbat-Plantey, K. Schädler, G. Navickaite, L. Gaudreau, F. S. Cataliotti, and F. Koppens, New J. Phys. **16**, 113007 (2014).

[29] Y. Tian, P. Navarro, B. Kozankiewicz, and M. Orrit, Chem. Phys. Chem. **13**, 3510 (2012).

[30] P. Siyushev, G. Stein, J. Wrachtrup, and I. Gerhardt, Nature (London) **509**, 66 (2014).

[31] J. Hwang and E. A. Hinds, New J. Phys. **13**, 085009 (2011).

[32] D. Wang, H. Kelkar, D. Martin-Cano, T. Utikal, S. Götzinger, and V. Sandoghdar, Phys. Rev. X **7**, 021014 (2017).

[33] N. R. Verhart, M. Müller, and M. Orrit, Chem. Phys. Chem. **17**, 1524 (2016).

[34] F. Jelezko, P. Tamarat, B. Lounis, and M. Orrit, J. Phys. Chem. **100**, 13892 (1996).

[35] C. Hofmann, A. A. L. Nicolet, M. A. Kol'chenko, and M. Orrit, Chem. Phys. **318**, 1 (2005).

[36] A. A. L. Nicolet, M. A. Kol'chenko, C. Hofmann, B. Kozankiewicz, and M. Orrit, Phys. Chem. Chem. Phys. **15**, 4415 (2013).

[37] S. Grandi, K. D. Major, C. Polisseni, S. Boissier, A. S. Clark, and E. A. Hinds, Phys. Rev. A **94**, 063839 (2016).

[38] A. Makarewicz, I. Deperasinska, E. Karpiuk, J. Nowacki, and B. Kozankiewicz, Chem. Phys. Lett. **535**, 140 (2012).

[39] B. Kozankiewicz and M. Orrit, Chem. Soc. Rev. **43**, 1029 (2014).

[40] National Center for Biotechnology Information, Pubchem Compound Database, cid=135991, 2018, https://pubchem.ncbi.nlm.nih.gov/compound/135991.

[41] R. Englman and J. Jortner, Mol. Phys. **18**, 145 (1970).

[42] C. M. Marian, WIREs Comput. Mol. Sci. **2**, 187 (2012).

[43] J. D. Coyle, *Introduction to Organic Photochemistry* (Wiley, New York, 1989).

[44] I. Deperasinska, E. Karpiuk, M. Banasiewicz, and B. Kozankiewicz, Chem. Phys. Lett. **492**, 93 (2010).

[45] M. B. Smith and J. Michl, Annu. Rev. Phys. Chem. **64**, 361 (2013).

[46] Z. S. Sadeq and J. E. Sipe, arXiv:1511.09396.

[47] C. Raghu, Y. Anusooya Pati, and S. Ramasesha, Phys. Rev. B **65**, 155204 (2002).

[48] J. Hachmann, J. Dorando, M. Aviles, and G. K.-L. Chan, J. Chem. Phys. **127**, 134309 (2007).

[49] I. Hagymási and O. Legeza, Phys. Rev. B **94**, 165147 (2016).

[50] J. Fabian, L. A. Diaz, G. Seifert, and T. Niehaus, J. Mol. Struct.: THEOCHEM **594**, 41 (2002).

[51] L. Serrano-Andrés and M. Merchán, J. Mol. Struct.: THEOCHEM **729**, 99 (2005).

[52] Y. X. Yao, J. Liu, C. Liu, W. C. Lu, C. Z. Wang, and K. M. Ho, Sci. Rep. **5**, 13478 (2015).

[53] Z. S. Sadeq, R. A. Muniz, and J. E. Sipe, Phys. Rev. Mater. **2**, 014001 (2018).

[54] W. Barford, *Electronic and Optical Properties of Conjugated Polymers*, 1st ed. (Oxford University Press, New York, 2005).

[55] R. Pariser and R. G. Parr, J. Chem. Phys. **21**, 466 (1953).

[56] R. Pariser and R. G. Parr, J. Chem. Phys. **21**, 767 (1953).

[57] J. A. Pople, Proc. Phys. Soc. **68**, 81 (1954).

[58] J. Vergés, G. Chiappe, and E. Louis, Eur. Phys. J. B **88**, 200 (2015).

[59] R. Kundu, Mod. Phys. Lett. B **25**, 163 (2011).

[60] W. Barford, R. J. Bursill, and M. Y. Lavrentiev, J. Phys.: Condens. Matter **10**, 6429 (1998).

[61] I. Ozfidan, M. Korkusinski, A. D. Güçlü, J. A. McGuire, and P. Hawrylak, Phys. Rev. B **89**, 085310 (2014).

[62] B. J. Powell, Introduction to effective low-energy Hamiltonians in condensed matter physics and chemistry, in *Computational Methods for Large Systems: Electronic Structure Approaches for Biotechnology and Nanotechnology*, edited by J. R. Reimers (Wiley, New York, 2011), pp. 309–366.

[63] K. Aryanpour, A. Roberts, A. Sandhu, R. Rathore, A. Shukla, and S. Mazumdar, J. Phys. Chem. C **118**, 3331 (2014).

[64] R. W. Boyd, *Nonlinear Optics* (Academic Press, San Diego, 2008), p. 166.

[65] R. W. Boyd, *Nonlinear Optics* (Academic Press, San Diego, 2008).

[66] R. W. Boyd, *Nonlinear Optics* (Academic Press, San Diego, 2008), p. 183.

[67] J. Wei, *Nonlinear Super-Resolution Nano-Optics and Applications* (Springer, New York, 2015).

[68] R. W. Boyd, *Nonlinear Optics* (Academic Press, San Diego, 2008), p. 169.

[69] K. Dolgaleva, R. W. Boyd, and P. W. Milonni, J. Opt. Soc. Am. B **24**, 516 (2007).

[70] K. Dolgaleva and R. W. Boyd, Adv. Opt. Photon. **4**, 1 (2012).

[71] T. Basché, S. Kummer, and C. Bräuchle, Excitation and emission spectroscopy and quantum optical measurements, in *Single-Molecule Optical Detection, Imaging and Spectroscopy*, edited by T. Basché, W. E. Moerner, M. Orrit, and U. P. Wild (VCH Verlagsgesellschaft mbH, Berlin, 2007), pp. 31–67.

[72] J. J. Sakurai, *Modern Quantum Mechanics* (Addison-Wesley, New York, 1994).

[73] A. S. Clark, S. Boissier, C. Polisseni, S. Grandi, K. Major, and E. A. Hinds, *Advanced Photonics 2016 (IPR, NOMA, Sensors, Networks, SPPCom, SOF)* (Optical Society of America, New York, 2016), p. IW3B.6.

[74] D. J. Tannor, *Introduction to Quantum Mechanics: A Time-Dependent Perspective* (University Science Books, Sausalito, 2006).